MDPI

Article

ENCODING GEOMETRIC FRUSTRATION IN TETRAHEDRAL PACKING WITH GAPS, DISCRETE CURVATURE, DISTORTION OR TWISTING

Fang Fang [1]*, Richard Clawson [1,2] and Klee Irwin [1]

[1] Quantum Gravity Research, Los Angeles, CA, U.S.A.
[2] University of Southern Queensland, Queensland, Australia
* Correspondence: fang@quantumgravityresearch.org

Academic Editor: name
Version March 23, 2017 submitted to Crystals

Abstract: This paper presents various ways of encoding *geometric frustration* in tetrahedral packings, by introducing small gaps to form quasicrystalline order, by curving to the 4th dimension with discrete curvatures, by distortion of tetrahedral edges and by twisting the edge-sharing and/or vertex-sharing local tetrahedral clusters. The key to these methods is to encode the deficit of the tetrahedral dihedral angle in closing a circle which is the cause of the geometric frustration. A surprising connection between the *discrete curvature* method and the *twisting* method is that both the *transformation angle* and the *joint angle* are the same in the one case as in the other. This connection leads to a way of encoding discrete curvature with twisting, which may help to model spacetime based on a quasicrystalline network that serves as a discrete version of a pseudo-Riemannian space.

Keywords: Geometric frustration; discrete curvature; twisting, tetrahedral packings; Clifford algebra; effective dihedral angle.

1. Introduction

Geometric frustration, as discussed in this paper, refers to situations where local order cannot propagate freely throughout space [1]. Classical examples include 2D pentagonal order and 3D icosahedral order, where the dihedral angle of the unit cell does not divide 2π, and therefore, it is not compatible with the translations. A traditional solution to relieve the frustration in nD is to curve the space into $n+1$D so that the vertices of the prototiles (pentagons in the 2D example) all land on an n-sphere (dodecahedron) and the discrete curvature is concentrated at the joints of the prototiles (dodecahedral edges). This eliminates the deficit in the dihedral angle to close a circle [1]. As in the above example, the pentagonal order can propagate freely on a 2-sphere, for example a dodecahedron or icosahedron, while the icosahedral order can propagate freely on a 3-sphere, for example, a 600-cell or 120-cell. However, the above hyper-sphere solution gives only a finite propagation of the local order since the spherical space is finite. In order to achieve infinite propagation, quasicrystalline order needs to be considered. There will be more rules/restrictions and complexity in the quasicrystal. Nevertheless, global propagation of the local pattern can be achieved.

This paper focuses on tetrahedral packings as an example. There has been a race on dense tetrahedral packings in recent years [2–9]. It is clear that the densest local tetrahedral cluster is 20 tetrahedra sharing a vertex, which forms local icosahedral order that cannot propagate freely, leading to geometric frustration. Various methods to propagate this local order and encode the geometric frustration are discussed in the following sections. Specifically, the surprising mapping of

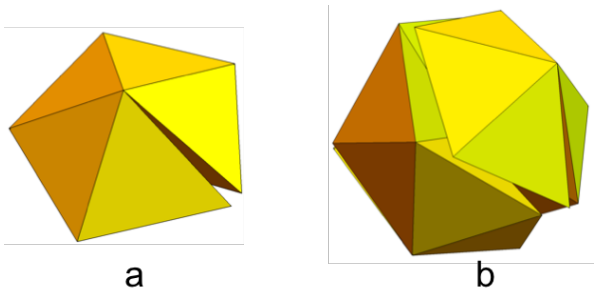

Figure 1. An (**a**) edge-sharing and (**b**) vertex sharing local tetrahedral cluster.

the *transformation angle* and *joint angle* between the *discrete curvature* method and the *twisting* method leads to a conjecture on representing a discretized pseudo-Riemannian spacetime with a family of quasicrystalline twist networks.

2. Encoding Geometric Frustration in Tetrahedral Packing

The tetrahedron configuration is the densest local sphere packing in 3D, and is also with the lowest energy state for four atoms. Yet tetrahedron cannot tile 3D space. The densest packing of tetrahedra is therefore a non-trivial problem that is of interest to chemists and physicists, as well as mathematicians. Regular tetrahedra, with a dihedral angle of $ArcCos[1/3]$ that does not divide 2π, will leave gaps between them when arranged in edge-sharing (Figure 1a) or vertex-sharing (Figure 1b) configurations. It is this kind of "discrepancy" that is called geometric frustration. "Frustration" here can also be thought of in some models as "pressure" or "defects" that function as resistance to the crystalline propagation of the local pattern. In this sense, it is not really a "negative" concept. Quite the contrary, from an information theoretic point of view it can be used to encode information, or in spacetime physics it may be used to encode gravity. More details will be discussed in section 10.

The geometric frustration in tetrahedral packings can be encoded in four different ways: 1) by evenly distributing the gaps, 2) by discrete curvature into a fourth dimension, 3) by distortion, and 4) by twisting. All these methods will enable quasicrystalline propagation of the local pattern. The following sections will introduce each method and the connections between them, mostly using the vertex-sharing 20-tetrahedron cluster as an example.

2.1. Encoding Geometric Frustration with Gaps

For the local cluster to have definite symmetry order, we choose to distribute the gaps evenly between the tetrahedra (Figure 2a) and le local icosahedral order propagate in quasicrystal by introducing other local order. This method of encoding geometric frustration is called the *gap* method, and the propagation of the local order using this method was demonstrated by Fang et.al. [10]. An icosahedral quasicrystal, as a packing of tetrahedra, can be obtained by two approaches: the first is by decorating a quasicrystal that is a 3D slice of the Elser-Sloane quasicrystal [11], and the second is by decorating the 3D Ammann tiling with regular tetrahedra [12].

The first approach is a guided decoration of the 3D slice of the Elser-Sloane quasicrystal, which contains three types of intermeshing polyhedra, icosidodecahedra, dodecahedra, and icosahedra, as shown in Figure 3a. These polyhedra are decorated (Figure 3c-e) based on the arrangement of the tetrahedra in the 600-cells of the Elser-Sloan quasicrystal because each of the shapes is a section (boundary of a *cap*) of a 600-cell. For example, the dodecahedron is a slice above the equator of the 600-cell and is the boundary of a cap of 70 tetrahedra. This is why the dodecahedron is decorated with 70 tetrahedra, as shown in Figure 3e. For the icosidodecahedron, which is a slice through the equator of the 600-cell and is a cap of 300 tetrahedra, the outer layer of tetrahedra has to be removed

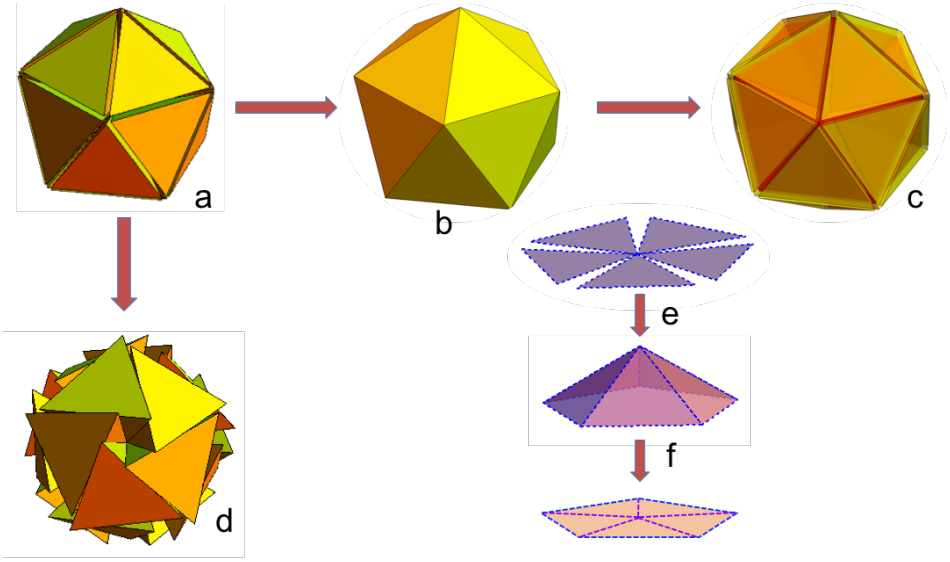

Figure 2. Four methods of encoding the geometric frustration in the 20-tetrahedron cluster: (**a**) by gaps, (**b**) by discrete curvature, (**c**) by distortion, and (**d**) by twisting. (**e**) → (**f**) illustrate the 2D analogy of the process of transitioning from the gaps to discrete curvature and then to distortion.

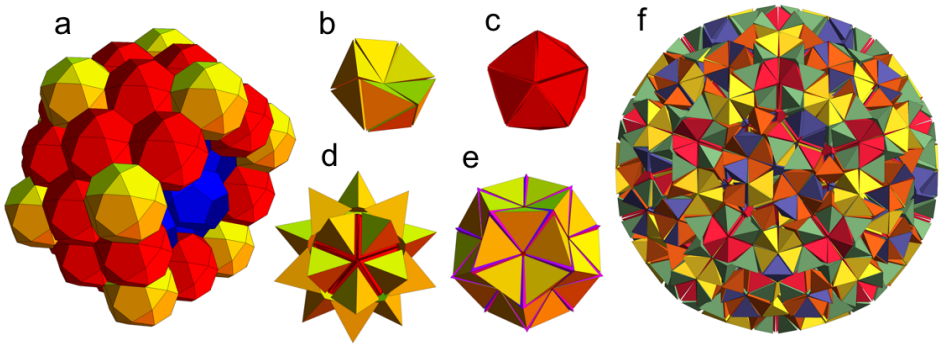

Figure 3. (**a**) 3D slice of the Elser-Sloane quasicrystal. (**b**) 10-tetrahedron "ring". (**c**) 20-tetrahedron "ball" (icosahedral cluster), obtained by capping the ring with two 5-tetrahedron groups. (**d**) 40-tetrahedron cluster, obtained by placing a tetrahedron on top of each face of the icosahedron in (**c**). (**e**) 70-tetrahedron dodecahedral cluster, obtained by adding 30 more tetrahedra in the crevices in (**d**). (**f**) Patch of the resulting quasicrystal, which contains the clusters shown in (**c**), (**d**) and (**e**) around its center.

to be able to fit nicely in the icosidodecahedron. This method can be thought of as a decoration of the 3D slice of the Elser-Sloane quasicrystal, guided by the structure of the quasicrystal itself.

The second approach is a direct decoration of the 3D Ammann tiling [12] generated by placing a 20-tetrahedron "ball" (Figure 3c) at each vertex, and a 10-tetrahedron "ring" (Figure 3b) around each edge of each of the rhombohedra, and then removing all those tetrahedra that do not intersect the rhombohedron. Like in the first approach, where the extra tetrahedra that do not fit have to be removed, here some tetrahedra at the facets of the rhombohedral cell have to pick a polarity to favor one of the two cells that share this facet.

In this quasicrystal, the geometric frustration is encoded in the finite types of gaps which preserve the icosahedral symmetry globally, as well as locally at certain vertices. Not all vertices in a quasicrystal have global symmetry, though, so it is not an ideal solution to express the geometric

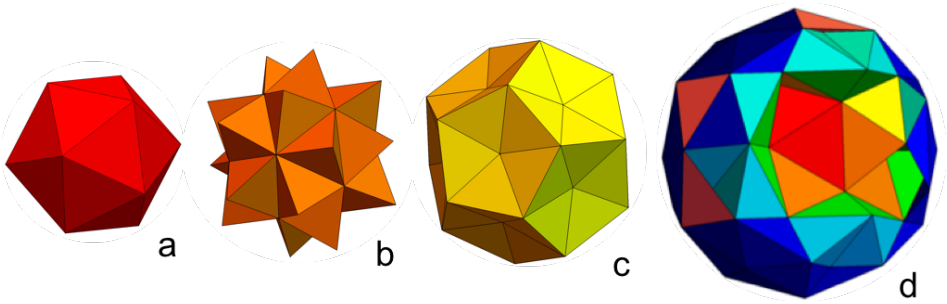

Figure 4. A sample patch of (**d**) the projected 3D quasicrystal, with (**a**) its first layer, (**b**) second layer and (**c**) third layer.

frustration from an energetic or ordering simplicity point of view. However, the extra complexity in the quasicrystal may have a useful application for encoding complex information.

2.2. Encoding Geometric Frustration with Discrete Curvature

An ideal solution to geometric frustration in tetrahedral packings is to use discrete curvature, where, unlike in the gap method, propagation of the local pattern is unhindered and all vertices are free of imperfect local symmetries. However, this method requires an extra dimension. For example, the 20-tetrahedron cluster in the configuration of Figure 2a can be bent into the 4th dimension to close all the gaps between tetrahedra, while keeping their shared vertex invariant, as shown in Figure 2b. (An analogue from 2D to 3D is shown in Figure 2e.) The angle by which each tetrahedron has to bend may be referred to as the *transformation angle*, and it may be positive or negative, corresponding to bending up or down in the 4th dimension. Where two faces close the gap and meet, geometric frustration is encoded in the dihedral angle between them, which we call the *joint angle*.

The vertices of the resulting 20-tetrahedron cluster belong to a 3-sphere that lives in 4D. This local icosahedral pattern can propagate freely on this 3-sphere until it forms a 4D polytope, the 600-cell, each of whose 120 vertices is surrounded by a 20-tetrahedron cluster in the configuration of Figure 2b. Therefore, a perfect match between local and global order is achieved. However, one drawback of this solution is that the 3-sphere is finite. It is true that the local order can propagate freely but not in infinite space. One way to resolve this limitation is to again introduce quasicrystalline order, which requires that extra local order to be added to the structure. Before we introduce this quasicrystal, let us start with the Elser-Sloane quasicrystal, a 4D cut-and-project of the E_8 lattice.

The Elser-Sloane quasicrystal can be thought of as a network of intermeshing 600-cells with a certain scale invariance whereby the whole structure repeats indefinitely at different scales. In this space, the order described above (the 20-tetrahedron clusters curved in 4D) can propagate by following partway along the surface of one 600-cell, then moving to a neighboring 600-cell at the joint between the two, while keeping this process up indefinitely, jumping from cell to cell through the 4D space. If we limit the path of the propagation to be within a distance of the radius of a 600-cell from a single Euclidean 3-space (*central 3-space*), then the whole path will cover a corrugated 3-space, with an aperiodic distribution of local curvature, which in turn encode the geometric frustration. Notice that in some places the order might not be able to propagate freely from one 600-cell to the next. In this case, extra local order will be introduced, as in the above gap method.

This quasicrystal that lives in a corrugated 3-space is the foundation for the next method, the *distortion* method.

2.3. Encoding Geometric Frustration with Distortion

Geometric frustration can be encoded by directly projecting the above quasicrystal into the central 3-space. Notice that this central 3-space is a slice of the Elser-Sloane quasicrystal that has

icosahedral symmetry, like the 3D slice mentioned in the gap method. Figure 4d shows a small patch of this projection, an icosahedral quasicrystal. There are 7 types of tetrahedra in Figure 4d and they are all projected from one 600-cell. Figure 4a shows the center 20 tetrahedra in the 600-cell projection. This process is illustrated in Figure 2b to Figure 2c and a 2D analogue is shown in Figure 2f. In Figure 2c, we see the edge distortion of the 20 red tetrahedra (in the projected quasicrystal) compared to the yellow regular tetrahedra in the 600-cell. The various degrees of distortion in this projected 3D quasicrystal encode both the information of the geometric frustration and the position of a given tetrahedron relative to the center point of the projection of the 600-cell to which it belongs. One should also be aware that there are other projected tetrahedral shapes at the positions where distinct 600-cells intersect in 4D.

2.4. Encoding Geometric Frustration with Twisting

The last method of encoding geometric frustration covered in this paper is by twisting the tetrahedra to close the gaps between neighboring tetrahedral faces. This method is important due to a unique correspondence with the discrete curvature method. Details of this mapping will be discussed in the next section. Let us again start with the 20-tetrahedron cluster. Fang *et al.* [13] have shown that the gaps can be closed by a twisting process from configuration 2a to configuration 2d, that is, a rotation of each tetrahedron around an axis that passes through the central shared vertex and the tetrahedron's opposing face center. The angle of twist needed to bring the faces together is called the *transformation angle*, and it can be positive or negative, resulting in either a left- or right-handed twisted cluster. Where the facets touch, they do not have the same orientation within their shared plane, and geometric frustration is encoded in the relative angle between them, which we call the *joint angle*.

The resulting configuration 2d has a similarity to configurations 2b and 2c in that all three configurations have their plane classes [14] reduced from 70 in 2a to the minimum number of 10, while maintaining the icosahedral symmetry. This similarity enables a similar quasicrystalline propagation of the local order of configuration 2d. One way to achieve this is to apply a similar twisting action to every tetrahedron in the quasicrystal used in the gap method, the result of which is shown by Fang *et al.* [10]. The second method is shown in another paper that is pending publication [13].

3. The Isomorphism between the Curving Method and the Twisting Method

For the two different methods of discrete curvature (section 2.2) and twist (section 2.4), we have defined the transformation angle and the joint angle for encoding geometric frustration. Surprisingly, we find that for the 20-tetrahedron cluster, both the transformation angle and the joint angle are exactly the same in the one case as in the other. (Note that the transformation angle equals to the angle of R. Buckminster Fuller's jitterbug rotation [15].) This perfect angle matching between the twisted tetrahedral clusters and the clusters on the 3-sphere are intriguing and motivate further study of similar cases. Regular tetrahedra can be arranged about a single, shared edge in clusters of 2-, 3-, 4- or 5-fold symmetry, and in each case the gaps between them can be closed either by bending up to 4D or by twisting in 3D. (In what follows, we ignore the 2-fold cluster because it is degenerate, though technically the results still apply.) The twisting is illustrated in the first two rows of Table 1.

To each edge-sharing cluster there corresponds a vertex-sharing cluster that preserves the relative orientations of the tetrahedra and the axial symmetry. Table 1 shows that the twisted 20-tetrahedron cluster, denoted as 20G, is a composition of twisted vertex-sharing 5-fold cluster and the vertex-sharing 3-fold cluster is a subset of this 20G. Furthermore, the twisted vertex-sharing 4-fold cluster has eight tetrahedra, with four in one orientation corresponding to a subset of the left-handed 20G and the other four in the other orientation corresponding to a subset of the right-handed 20G. It is not hard to realize that the 3-fold and 5-fold clusters have quasicrystalline order while the 4-fold has crystalline order.

Table 1. Categorizing the properties of three different types of tetrahedral local clusters and their corresponding 4D polyhedra.

Cluster types	**3-fold**	**4-fold**	**5-fold**
Evenly spaced edge-sharing	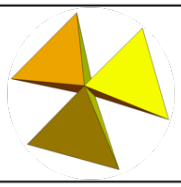	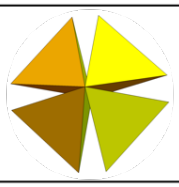	
Twisted edge-sharing	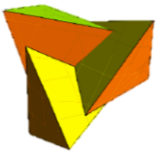		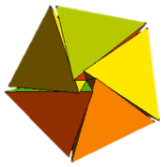
Twisted vertex-sharing	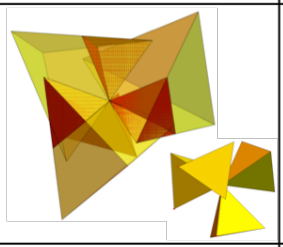	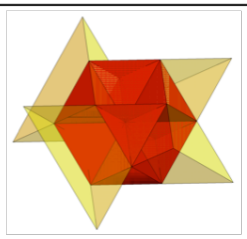	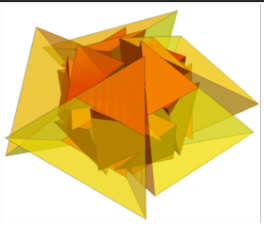
As a subset of 20G	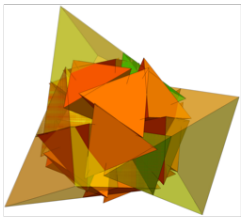	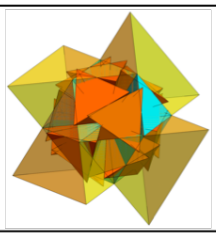	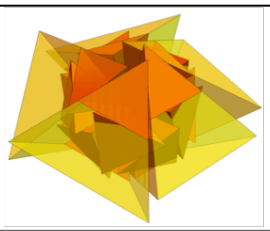
Twisting angles	E: $ArcCos\left(\frac{1}{\sqrt{6}}\right)$ V: $ArcCos\left(\frac{1}{4}\right)$ F: $ArcCos\left(\frac{1}{4}\right)$	E: $\frac{\pi}{4}$ V: $\frac{\pi}{3}$ F: $\frac{2\pi}{3}$	E: $ArcTan\left(\frac{1}{\phi^3}\right)$ V: $ArcCos\left(\frac{\phi^2}{2\sqrt{2}}\right)$ F: $ArcCos\left(\frac{1}{4}\right) - \frac{\pi}{3}$
4D analogue and angles	5-cell B: $ArcCos\left(\frac{1}{4}\right)$ D: $ArcCos\left(\frac{1}{4}\right)$	16-cell B: $\frac{\pi}{3}$ D: $\frac{2\pi}{3}$	600-cell B: $ArcCos\left(\frac{\phi^2}{2\sqrt{2}}\right)$ D: $ArcCos\left(\frac{1}{4}\right) - \frac{\pi}{3}$

As mentioned, both the transformation angle and the joint angle are identical, whether used to translate geometric frustration in a vertex-sharing 20-tetrahedron cluster from gaps to twisting or from gaps to discrete curvature. Therefore, we refer to the 600-cell as a 4D analogue of the 20G due to this isomorphism between these two transformations, as well as the fact that in both cases the number of tetrahedra sharing a common edge (or edge center) is five, and the number of tetrahedra sharing a common vertex is 20. Similarly, the 16-cell is the 4D analogue of the 4-fold case, and the 5-cell is the 4D analogue of the 3-fold case. In the twisting angle row of Table 1, "E" denotes the twisting angle of the tetrahedron around an axis connecting the midpoints of its central and peripheral edges to close the edge sharing cluster, "V" denotes the transformation angle to close the vertex-sharing cluster, and "F" denotes the joint angle. For the angles in the 4D analogues, "B" denotes the transformation angle

(the bending angle to close the gaps) and "D" the joint angle (dihedral angle in this case). Notice that, in all three cases, both the transformation angle and the joint angle match exactly! This finding implies that, at least locally, there is a perfect equivalence between encoding geometric frustration using the discrete curvature method and the twisting method, in other words, the discrete curvature in 4d can be replaced by the twisting in 3D because, in either case, the information is encoded in these matching angles.

4. Geometry of closing the gaps

In all the three cases other than the gaps, there is a manipulation on the dihedral angle to close the deficit angle to achieve face kissing and parallel plane class reduction. Fig. 5b-d shows the methods of twisting, curvature and distortion to enlarge the *effective dihedral angle* (projection of the dihedral angle in the central plane, colored light blue in the figure) and thereby close up the gaps in Fig. 5a. Both the twisting method (Fig. 5b) and the curvature method (Fig. 5c) achieve the goal by rotating the tetrahedral dihedral angle (enclosed by the red vectors) out of the central plane which results in the corresponding effective dihedral angle in the plane becoming larger.

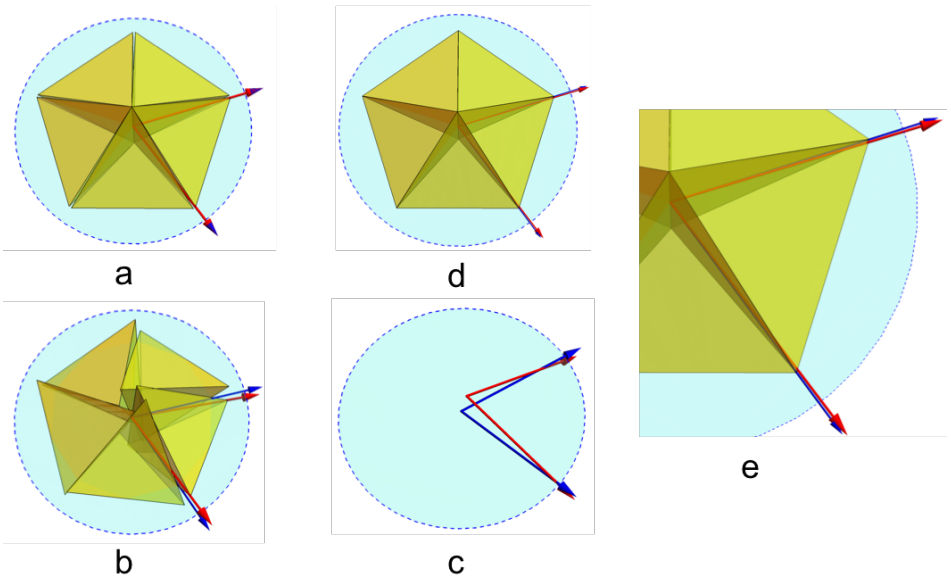

Figure 5. Illustration of three different processes of manipulating the tetrahedral dihedral angle in order to remove the deficit angle in the 5-tetrahedron edge-sharing cluster. The red vectors always enclose the tetrahedral dihedral angle and the blue vectors enclose the effective dihedral angle ($2\pi/5$) on the central plane (light blue) to close the gaps. (**a**) 5 tetrahedra sharing a center edge with gaps/deficit angle evenly distributed between tetrahedra. The gaps are eliminated through (**b**) twisting each tetrahedron in the way described above, (**c**) bending the tetrahedra to the 4th dimension, or (**d**) distortion of the tetrahedral edge length. (**e**) is a magnified view of (**d**) which shows the difference between the two angles that is hard to see when they are on the same plane.

5. Proofs of Angle Matching between Discrete Curvature and Twist

In the following sections, we give technical proofs of the angle matching between the discrete curvature and twist cases. Proofs can be done with multiple step trigonometry, but here we use Clifford algebra. We do so because Clifford algebra is fundamentally a geometric language. It facilitates articulating the proofs by providing a clean and efficient algebraic encoding of geometric concepts. Indeed, it is often referred to simply as *geometric algebra*. For the reader unfamiliar with it, [16–18] provide useful introductions, [19] gives a briefer introduction with application to the crystallographic space groups, and [20,21] are two monograph references.

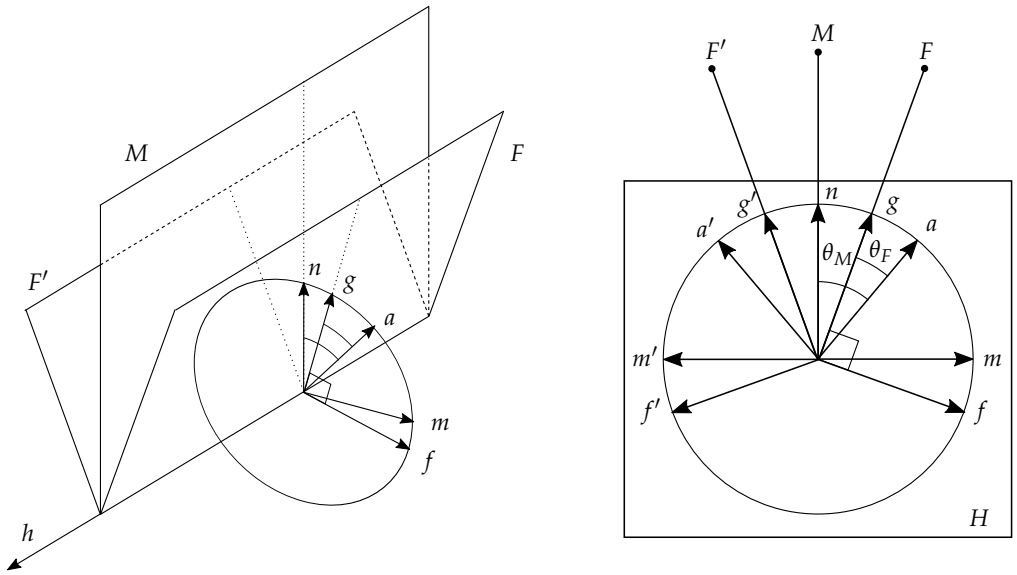

Figure 6. Face planes F and F', symmetric across a mirror plane M. They share a common vector h, and have normals f and f'. Shown (**a**) obliquely and (**b**) directly from the $+h$ direction.

The curve and the twist are orthogonal transformations in 4 and 3 dimensions, respectively, that bring the faces F of adjacent tetrahedra into contact. We begin with some general considerations on bringing two distinct bivector planes into coincidence by such rotations. After that we shall apply the resulting formulas to the cases of interest involving tetrahedra in the edge-sharing and vertex-sharing configurations.

Transformations between Bivectors – Basic Definitions

Given any two intersecting planes F and F' in 3D, there is a unique mirror plane M through which F' is a reflection of F. We represent these planes by bivectors, shown in Figure 6, along with the bivector H orthogonal to them all. The following vectors are also introduced. Let h be the vector normal to H, along the intersection of F, F', and M. Let m and f be normal to M and F, respectively, and on the same side, and let $g = fH$, $n = mH$, so that f, g, h and m, n, h are right-handed orthogonal vector triads. Let all these vectors and bivectors have unit magnitude (though in the figure, for visual clarity, the bivectors are shown enlarged). Furthermore, let i be the unit right-handed trivector of the space. Thus,

$$\begin{gathered} m^2 = -M^2 = 1, \text{ etc.} \\ M = im, \quad F = if, \quad H = ih, \\ fgh = mnh = i = \text{unit 3D trivector.} \end{gathered} \tag{1}$$

We include an additional unit vector a which will be used to construct the transformations. Finally, each multivector is paired with its mirror reflection through M, denoted by a prime symbol, e.g., F' is the reflection of F, f' that of f, etc. (a is an exception—its counterpart a' is across M, but is not necessarily a reflection.)

The bivector F' can be brought into coincidence with F by either the discrete curve or the twist transformation as described in the previous sections. Each of these is a rotation characterized by a

simple bivector (its rotation plane), and the vector a is introduced to define these bivectors—in the curve case a is part of the rotation plane, and in the twist case it is the rotation axis. Along with a we have defined θ_M and θ_F, the angles that a makes respectively with the mirror M and the face F. (Note that in the figure, we have drawn a in the H-plane: that is a case of particular interest, which simplifies some results and is necessary for others, but the derivations below will not assume it to begin with. It turns out to be necessary when a' is the mirror reflection of a.)

6. Transformation Angles

6.1. Discrete Curvature – Rotation from a to e_4 in the 4th Dimension

As indicated in the section on encoding geometric frustration by discrete curvature, the faces F and F' can be brought together by rotating each up into the fourth dimension. Let e_4 be the unit vector in 4D orthogonal to i. We rotate F in the e_4a plane and F' in the e_4a' plane, so the two rotations come from different lines in 3D but converge toward the same line in the fourth dimension. The rotations are symmetric across the mirror plane M—or, more accurately, they are symmetric across the hypersurface normal to m. For each multivector, therefore, we define its counterpart as its reflection in this hypersurface,

$$a' = -mam, \quad F' = mFm, \quad \text{etc.} \tag{2}$$

(plus sign for even multivectors, minus sign for odd ones). Each rotation acts on the entire 3D space, and so each rotates the initial space i into a distinct space. They do this in such a way that F and F' are brought together where the two spaces intersect in a sort of fold of discrete curvature (the 2D-to-3D analogue is illustrated in Figure 2e). The transformations are given by

$$\begin{aligned} F &\to F_c = CF\widetilde{C} \qquad C = e^{\frac{1}{2}e_4a\alpha} \\ F' &\to F'_c = C'F'\widetilde{C}' \qquad C' = e^{\frac{1}{2}e_4a'\alpha}, \end{aligned} \tag{3}$$

where α is the angle of rotation, and reversion of C is represented by the tilde, $\widetilde{C}$. With a' given by (2), the rotation bivector for C' becomes $e_4a' = -e_4mam = me_4am$, so C' is

$$C' = e^{m(\frac{1}{2}e_4a\alpha)m} = mCm. \tag{4}$$

Now as F' is rotated, it becomes

$$F'_c = C'F'\widetilde{C}' = mCmmFmm\widetilde{C}m = mCF\widetilde{C}m = mF_cm, \tag{5}$$

so F'_c and F_c are still related by reflection. Convergence, then, means that F_c has become its own reflection, i.e.,

$$F_c = F'_c = mF_cm. \tag{6}$$

This implies F_c is orthogonal to m, or

$$0 = \langle F_cm \rangle_1 = \left\langle CF\widetilde{C}m \right\rangle_1, \tag{7}$$

where $\langle \dots \rangle_k$ means the k-vector part of the expression (in this case, the 1-vector part, i.e., the vector part). Eq. (7) can be expanded by splitting F into parts that commute and anticommute with a,

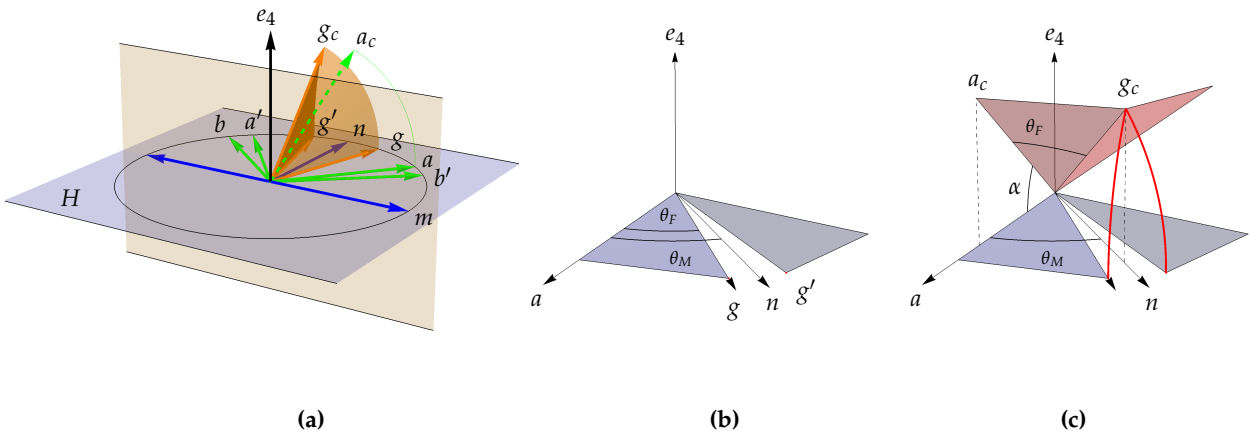

(a) **(b)** **(c)**

Figure 7. Aspects of the curvature transformation, shown in the He_4 3-space. (**a**) Vectors g and g' rotate respectively around b and b', to where they meet in the ne_4 plane. Vector a also rotates up to a_c, so θ_F between a_c and g_c projects down to θ_M between a and n. (**b**), (**c**) Alternative view, showing how θ_F, after the rotation, projects to match θ_M in the H plane

$$F_+ \equiv F \wedge aa, \quad F_- \equiv F \cdot aa, \quad F = F_+ + F_- \tag{8}$$

$$CF_+\widetilde{C} = F_+, \qquad CF_-\widetilde{C} = C^2F_-. \tag{9}$$

(We have used the fact that all bivectors in 3D commute with e_4, so since F_+ commutes with a it also commutes with e_4a. In like manner F_- anticommutes with e_4a.) We use this expansion in (7), and expand $C^2 = e^{e_4a\alpha}$ into $\cos\alpha + e_4a\sin\alpha$. This yields

$$\begin{aligned} 0 &= \left\langle CF\widetilde{C}m \right\rangle_1 = \left\langle F_+m + C^2F_-m \right\rangle_1 \\ &= F_+ \cdot m + \cos\alpha F_- \cdot m + \sin\alpha \left\langle e_4aF_-m \right\rangle_1 \\ &= F_+ \cdot m + \cos\alpha F_- \cdot m + e_4 \sin\alpha\, a \cdot F \cdot m. \end{aligned} \tag{10}$$

The last step is because e_4 is perpendicular to the 3-space that contains F_+, F_-, and m, and for the same reason, the last term is orthogonal to the first two and so must vanish independently. Ignoring the trivial case of $\alpha = 0$, this means

$$0 = a \cdot F \cdot m = F \cdot m \wedge a, \tag{11}$$

and so in order for us to have a solution, the $m \wedge a$ plane must be perpendicular to F, or, looking at Figure 6, a must lie in H. This eliminates the $\sin\alpha$ term in (10), which can then be solved for

$$\cos\alpha = -\frac{F_+ \cdot m}{F_- \cdot m} = -\frac{\left\langle F \wedge a\, am \right\rangle_1}{\left\langle F \cdot a\, am \right\rangle_1} = \frac{F \wedge a\, m \wedge a}{F \cdot a\, m \cdot a}, \tag{12}$$

where the denominator was simplified using the fact that $F \cdot a$ is orthogonal to both a and m. Looking again at Figure 6 we can write this in terms of the angles,

$$\cos\alpha = \frac{\sin\theta_F \cos\theta_M}{\cos\theta_F \sin\theta_M} = \frac{\tan\theta_F}{\tan\theta_M}. \tag{13}$$

One can understand the geometry of this calculation with the help of Figure 7. Since h is left invariant, we ignore it for now and consider the 3-space of He_4. Figure 7a shows how as a is rotated

up toward e_4, it traces out a disc with axis b, and its projection down in H stays along a. Meanwhile, g is also rotated around b, tracing out a cone. It meets g' where that cone intersects the ne_4 plane, whereupon $g_c \perp m$, so F_c ($= g_c h$) is orthogonal to m, which is the constraint (6) that determines our solution.

At that point, the projection of g_c down in H lies along n, so θ_F between g_c and a_c projects down to θ_M between n and a (Figure 7c). For tetrahedra arranged symmetrically about a shared edge, the gap $2(\theta_M - \theta_F)$ between face planes is the angular deficit, and the projective matching of θ_F to θ_M eliminates this deficit and closes the circle.

6.2. Twist – Rotation about a in 3D

Instead of using rotations from a and a' into the 4th dimension, we may bring F and F' into coincidence by rotating them *around* the a and a' axes in 3D. In this case, referred to as the twist, both rotations are given the same handedness about their respective axes, rather than rotating in toward each other or out away from each other; they are not, therefore, mirror reflections of each other. As shown below, the primed rotation can be constructed from the unprimed one by inversion through the single vector n, which lies in the reflection plane M and is normal to the intersection line h (see Figure 6). F and F' are still related by mirror inversion through M, but since both F and n are perpendicular to H, this is equivalent to an anti-inversion through n. Thus,

$$\begin{aligned} a' &= ngn, \\ F' &= mFm = HnFHn = -nFn, \end{aligned} \tag{14}$$

$$\begin{aligned} F &\rightarrow \quad F_t = TF\widetilde{T} \qquad T = e^{-\frac{1}{2}ia\alpha} \\ F' &\rightarrow \quad F'_t = T'F'\widetilde{T}' \qquad T' = e^{-\frac{1}{2}ia'\alpha}, \end{aligned} \tag{15}$$

$$T' = e^{n(-\frac{1}{2}ia\alpha)n} = nTn. \tag{16}$$

where α is the transformation angle, as before. We justify using the same symbol as in the discrete curvature case by showing below that it has the same value.

As F' is transformed, it becomes

$$F'_t = T'F'\widetilde{T}' = nTn(-nFn)n\widetilde{T}n = -nTF\widetilde{T}n = -nF_tn. \tag{17}$$

Similar to what we saw in the case of bending in 4D, F and F' continue to be related by anti-inversion through n as they are rotated. Solution for the α that brings them into coincidence therefore requires that F become its own anti-inversion, i.e.,

$$F_t = F'_t = -nF_tn, \tag{18}$$

which means that F_t contains n, or

$$0 = F_t \wedge n = \langle F_tn \rangle_3 = \left\langle TF\widetilde{T}n \right\rangle_3. \tag{19}$$

As before, this can be expanded by splitting F into F_+ and F_-, which have the same commutation properties with T as they did with C,

$$TF_+\widetilde{T} = F_+, \quad TF_-\widetilde{T} = T^2F_-. \tag{20}$$

Using this in (19) and expanding $T^2 = \cos\alpha - ia\sin\alpha$ gives

$$\begin{aligned} 0 = \left\langle TF_0\widetilde{T}n \right\rangle_3 &= \left\langle F_+n + T^2F_-n \right\rangle_3 \\ &= F_+ \wedge n + \cos\alpha F_- \wedge n - \sin\alpha \left\langle iaF_-n \right\rangle_3 \\ &= F_+ \wedge n + \cos\alpha F_- \wedge n - i\sin\alpha\, a\cdot F\cdot n. \end{aligned} \tag{21}$$

In contrast to the previous case, all three terms here are linearly dependent, so the $\sin\alpha$ term does not vanish independently: a and a' need not lie in the H plane. Substituting for $\sin\alpha$ in terms of $\cos\alpha$, we could make of (21) a quadratic in $\cos\alpha$ with a straightforward but slightly messy solution. For our current purposes, however, we want to compare the transformation angle α in the twist case to that in the discrete curvature case, starting from the same initial configuration and using the same vectors a and a' to define the transformations. We therefore take a to lie in H as before. This once again eliminates the $\sin\alpha$ term, and (21) can be solved for $\cos\alpha$,

$$\cos\alpha = -\frac{F_+ \wedge m}{F_- \wedge m} = -\frac{\langle F\wedge a\, an\rangle_3}{\langle F\cdot a\, an\rangle_3} = \frac{F\wedge a\, n\cdot a}{F\cdot a\, n\wedge a}, \tag{22}$$

where the denominator in the last expression uses the fact that $F\cdot a$ is orthogonal to both a and n. Referring to Figure 6, we can write this in terms of the angles,

$$\cos\alpha = \frac{\sin\theta_F\cos\theta_M}{\cos\theta_F\sin\theta_M} = \frac{\tan\theta_F}{\tan\theta_M}. \tag{23}$$

This reproduces (13), demonstrating that in order to bring the face planes into coincidence, the twist transformation requires the same angle as the discrete curvature one.

It is a bit tricky to understand the geometry of this calculation by visualizing the rotations of the planes, but since it all occurs in 3D, we can focus on the rotations of their normals f and f' illustrated in Figure 8a. The vector normal to H is now h, and all aspects of the transformation remain within the 3-space of $Hh = i$. Vectors f and f' are to be rotated until they are directly opposite each other; for easier comparison with the discrete curvature, we show f and $-f'$ in the figure, which rotate until they become the same. They sweep out cones around a and $-a'$, respectively, becoming aligned where these cones intersect the original mh plane, i.e., when $f_t \perp n$. That implies F_t ($= g_th_t$) contains n, which is the constraint expressed algebraically by (19).

The twist also rotates g around a to g_t, keeping θ_F unchanged between g_t and a (Figures 8b,8c). F is rotated around a until F contains n (i.e., $f_t \perp n$), whereupon the projection of n onto H_t (dark red triangle) lies along g_t. Therefore, θ_M between n and a projects onto H_t to match θ_F between g_t and a. (Note that here we are comparing θ_M and θ_F as projected onto the twisted H_t, whereas in the discrete curvature case we compared the angles as projected onto the original H.) Figures 8b and 8c also include an extra plane F'' that forms a dihedral angle of $2\theta_F$ with F. One can see how, as the planes are rotated, that dihedral angle's cross section in the H plane (blue) expands to match $2\theta_M$.

6.3. Comparing Discrete Curvature and Twist

In the discrete curvature case, the g_c cone makes an angle $90^\circ - \theta_F$ with its axis b, and intersects the vertical ne_4 plane in two places. For the twist, f_t makes the same angle with its axis a, intersecting the vertical mh plane in two places. Clearly, the angle of rotation required along their respective cones to bring g_c and f_t to their respective intersections is the same. This shows geometrically that the transformation angle α is the same for both C and T.

We also think of this in terms of the angles θ_F and θ_M. Both C and T rotate g until it is projectively aligned with n. The respective rotation planes ae_4 and bh are accompanied by different projections, the one into H and the other into H_t, but the effect in both cases is that, in the projection, θ_F is made to match θ_M and the angular deficit is eliminated.

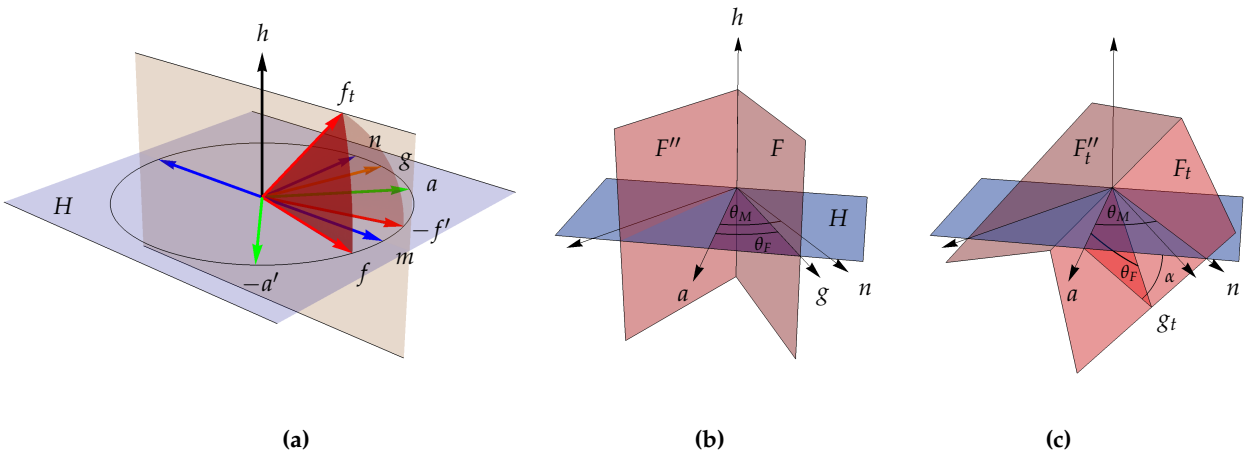

Figure 8. Aspects of the twist transformation, in the Hh 3-space. (**a**) Vectors f and $-f'$ rotate respectively around a and $-a'$, to where they meet in the mh plane. (**b**), (**c**) Alternative view, showing plane F (instead of its normal f) along with F'' to exhibit the dihedral angle $2\theta_F$. Vector g rotates around a down to g_t until θ_M between n and a projects in H_t to θ_F between g_t and a. Within the H plane, the effective dihedral angle has expanded from θ_F to θ_M.

Note, by the way, that (13) and (23) admit of both positive and negative solutions for α. In the discrete curvature approach, this corresponds to bending toward $\pm e_4$, while in the twist it corresponds to left- or right-handed rotation around a.

7. Joint Angles in the Final Configurations

The two face planes F and F' live initially in a single 3D space. We associate with each a unique trivector, $i = fgh$ and $i' = f'g'h$, where the primed vectors are mirror reflections across M. Because they are in the same 3-space, the two trivectors differ only by a sign, $i' = -i$, due to the reflection (you can see in Figure 6 that $f'g'h$ has the opposite handedness of fgh). The discrete curve and the twist are each constructed so as to bring the bivectors F and F' into coincidence, but they do not in general bring each individual vector into alignment with its primed counterpart. This results in what we have called the *joint angle* where the face planes meet.

Under the discrete curvature transformation, the two rotations C and C' have different actions on the original 3D space, so that $i'_c \neq -i_c$. More specifically, the vectors within F and F' do converge (g and g' are brought together in the final state, and $h = h'$ is left invariant), but the normal vector f does not become $-f'$, because along the $F = F'$ plane the two 3-spaces i and i' meet at a folded joint. The joint angle β is the dihedral angle between them, equivalent to the angle between f and f'.

Under the twist, the situation is reversed. T and T' leave i and i' invariant, so $F' = F$ implies that $f' = -f$. In this case, it is g' and h' that are twisted relative to g and h within the final F plane, and their relative angle is the joint angle for the twist transformation.

7.1. Joint Angle for Discrete Curvature in 4D

The dihedral angle β between the two trivectors curved up in 4D is equivalent to the angle between face normals f_c and $-f'_c$ (this is actually the exterior dihedral angle; its supplement is the interior angle, between f_c and $+f'_c$.). Because the rotations as well as the initial vectors are symmetric with respect to reflection by m, the transformed vectors are likewise mirror symmetric, so that m bisects the angle between f_c and $-f'_c$. It is actually simpler to calculate this half angle, so we calculate the inner product of f_c with m,

$$\cos\beta = (-f'_c)\cdot f_c, \qquad \cos\frac{\beta}{2} = m\cdot f_c. \tag{24}$$

We have an explicit expression for C, so it is straightforward to calculate $m \cdot f_c = \langle mCf\widetilde{C}\rangle$. There is, however, a slightly more direct path to the result. We found in Section 6.1 that $g_c \perp m$. Since any vector v_c in the H_c plane can be expanded in terms of g_c and f_c, its inner product with m is

$$m \cdot v_c = m \cdot f_c f_c \cdot v_c + m \cdot g_c g_c \cdot v_c = m \cdot f_c f_c \cdot v_c. \tag{25}$$

This allows us to solve for $m \cdot f_c$ in terms of v_c, whatever it may be. Among all the possible vectors in the H_c plane, b_c is of particular use because $b = b_c$ is invariant, being orthogonal to the rotation plane $e_4 a$. (Recall that $b = aH$; it is not shown in Figure 6, but can be seen in Figure 7a.) Thus,

$$m \cdot b = m \cdot b_c = m \cdot f_c \, f_c \cdot b_c = m \cdot f_c f \cdot b, \tag{26}$$

and therefore

$$\cos\frac{\beta}{2} = m \cdot f_c = \frac{m \cdot b}{f \cdot b} = \frac{\cos\theta_M}{\cos\theta_F}. \tag{27}$$

(In the last step we have used $m \cdot (-b) = n \cdot a = \cos\theta_M$ and $f \cdot (-b) = g \cdot a = \cos\theta_F$.)

7.2. Joint Angle for Twist in 3D

When the faces are twisted together in 3D, their internal frames g, h and g', h' end up rotated relative to each other by an angle β. (As with α, we shall justify reusing the label β by showing that it is the same as the β found in the previous section.) Once again the expression for the half angle is simpler, so we calculate the inner product of g_t with the vector midway between g_t and g_t'. The symmetry, however, is slightly different in this case because the two twist rotations T and T' are not mirror images across the plane M, but inversions through the vector n.

Now g' is the mirror reflection of g by m, but this is equivalent to inversion through n, because $-mgm = -HngHn = ngn$. Thus,

$$g' = ngn, \qquad a' = nan, \qquad T' = nTn, \tag{28}$$

which leads to

$$g_t' = T' g' \widetilde{T}' = nTnngnn\widetilde{T}n = ng_t n. \tag{29}$$

We therefore conclude that n is the vector midway between g_t and g_t', just as it is between g and g'. Hence,

$$\cos\beta = g_t' \cdot g_t, \qquad \cos\frac{\beta}{2} = n \cdot g_t. \tag{30}$$

As in the curve case, we can straightforwardly compute $n \cdot g_t = \langle nTg\widetilde{T}\rangle$, but there is a way that gives the desired expression more directly. For the twist, we found (Section 6.2) that $n \perp f_t$, so for any vector v_t in H_t,

$$n \cdot v_t = n \cdot g_t g_t \cdot v_t + n \cdot f_t f_t \cdot v_t = n \cdot g_t g_t \cdot v_t. \tag{31}$$

Since the twist rotation is in the ia plane, the invariant vector in H_t is $a = a_t$, and we dot with that to get

$$n \cdot a = n \cdot a_t = n \cdot g_t g_t \cdot a_t = n \cdot g_t g \cdot a. \tag{32}$$

This immediately gives a solution that matches (27) above,

$$\cos\frac{\beta}{2} = n \cdot g_t = \frac{n \cdot a}{g \cdot a} = \frac{\cos\theta_M}{\cos\theta_F}. \tag{33}$$

We thus find the joint angle β, like the transformation angle α, to be the same for both C and T.

8. Transformation between the Two Configurations—Mixed Curving and Twisting

[*** Maybe don't need this section.]

The two rotations C and T take place in the separate, non-intersecting planes e_4a and ia; the e_4a rotation leaves the ia plane invariant, and vice-versa. As a result, the combined transformation that takes the curved F_c directly to the twisted F_t can be written as a single exponential,

$$F_t = RF_c\widetilde{R} \tag{34}$$

$$R \equiv T\widetilde{C} = e^{-\frac{1}{2}ia\alpha}e^{-\frac{1}{2}e_4a\alpha} = e^{-\frac{1}{2}(e_4+i)a\alpha}. \tag{35}$$

The result is a compound rotation, occurring in two commuting bivector planes (a feature only found with dimension > 3). Likewise,

$$F'_t = R'F'_c\widetilde{R}' \tag{36}$$

$$R' \equiv T'\widetilde{C}' = e^{-\frac{1}{2}(e_4+i)a'\alpha}. \tag{37}$$

But $F'_t = F_t$, and $F'_c = F_c$, so the primed transformation actually has the same effect on F_c as the unprimed one,

$$R'F_c\widetilde{R}' = RF_c\widetilde{R}. \tag{38}$$

This is only true, however, for the angle α. For intermediate angles between 0 and α, the two transformations give different results so that, beginning with the face plane $F_c = F'_c$ in the fully curved state, the primed and unprimed transformations will take it through different intermediate states to reach the fully twisted configuration $F_t = F'_t$. Obviously, this must be so, since in the uncurved, untwisted configuration that was originally envisioned there are two distinct face planes.

One might ask if there are mixed transformations that bring F and F' together—a partial curve, followed by a partial twist, or vice versa. There are, but they involve some complications. After some curving, the 3-space of $F \wedge a$ is not the same as that of $F' \wedge a'$, so the rotated a and a' are not suitable axes for a twist. It can be shown that F and F' do inhabit a new, shared 3-space, and so twist axes can be found therein, but it does not seem sufficiently instructive to present details here.

9. Face-Sharing Tetrahedra

We now apply the results of Sections 6 and 7 to groups of tetrahedra which shall be brought together by our transformations so that they share certain face planes.

9.1. Shared Edge Configuration

Begin with a group of n congruent tetrahedra all having one edge in common, and oriented around that edge with uniform angular spacing (Figure 9). Define a_i to be the unit vector directed from the center of the shared edge out to the centroid of the ith tetrahedron (if continued, it will meet the center of that tetrahedron's opposite, outer edge). These a_i will all lie in a plane orthogonal to the shared edge, with angle $T = 2\pi/n$ between adjacent ones.

Each tetrahedron has the same dihedral angle D at the shared edge, and we suppose that $nD < 360°$, such that the tetrahedra do not fill the angular space around the edge, but leave gaps between their faces (By the way, for our transformations to have the desired effect, it is not strictly necessary

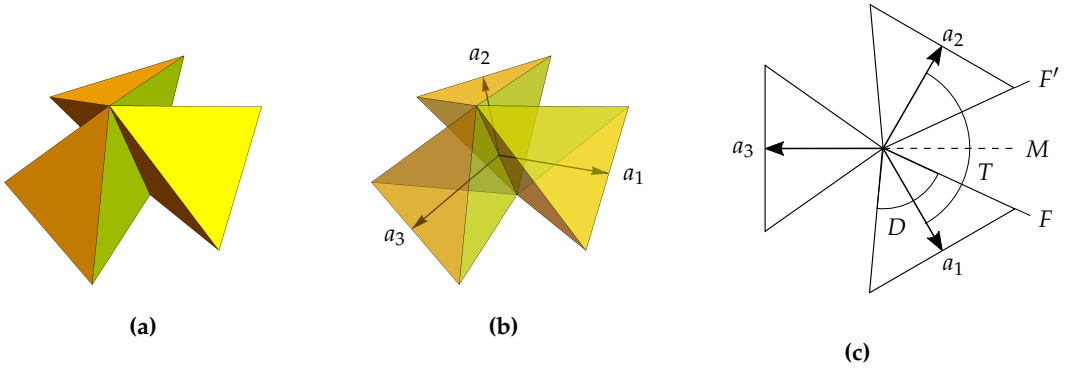

Figure 9. (**a**) Edge-sharing 3-Group, (**b**) including the a_i from the center of the shared edge out toward the centers of the respective opposite edges. (The unit vectors a_i are not to scale—the distance between the centers of two opposite edges is not necessarily a unit length.) (**c**) Overhead view showing the face planes F and F' that will be rotated into coincidence by the transformation (curve or twist) defined by a_1 and a_2.

that the tetrahedra be congruent, but only that their dihedral angles at this shared edge be congruent). Each vector a_i makes the same angle T with its neighbors $a_{i\pm1}$.

It is now clear that any two adjacent tetrahedra in the group have adjacent face planes whose line of intersection is the shared edge, and whose respective a_i are orthogonal to this edge. Midway between the two faces we can define a mirror plane M, and together with the two a_i (one in each tetrahedron) this provides the parameters for our transformation, whether the curve or the twist, which will bring those faces into contact. By comparing the figure with Figure 6 where we defined θ_M and θ_F, we see that

$$\theta_F = \frac{D}{2}, \qquad \theta_M = \frac{T}{2} = \frac{\pi}{n}. \tag{39}$$

Moreover, because the tetrahedra centroids are evenly spaced, the same angles apply to the faces on either side of each tetrahedron. Thus, a_2 will define the same transformation when paired with a_3 as with a_1. In this manner, a set of transformations defined by all the a_i and all the reflection planes will close all the gaps and bring all the faces into contact with their neighboring faces. Either the curve or the twist will do, each by the angle α found in the previous sections (eq. 13),

$$\cos\alpha = \frac{\tan(D/2)}{\tan(T/2)}. \tag{40}$$

After the transformation, the relative angle between adjacent faces, whether as a dihedral angle or as a twist, will be (eq. 27)

$$\cos\frac{\beta}{2} = \frac{\cos(T/2)}{\cos(D/2)}. \tag{41}$$

9.1.1. Regular Tetrahedra in Groups of 3, 4, or 5

For regular tetrahedra, the dihedral angle is given by $\cos D = \frac{1}{3}$. Arranged about their shared edge in groups of 3, 4, or 5, the respective angles between the a_i are $T_3 = 2\pi/3$, $T_4 = \pi/2$, and $T_5 = 2\pi/5$. This leads to the following transformation and face joint angles:

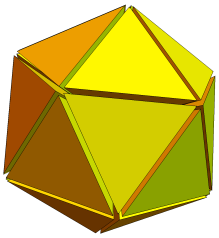

Figure 10. Vertex-sharing 20-tetrahedron cluster uniformly spaced, with gaps between all faces.

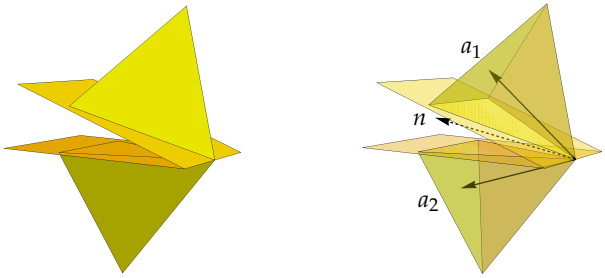

Figure 11. (**a**) Example of 2 vertex-sharing tetrahedra with their face planes, (**b**) showing their centroid axes a_i bisected by n.

$$\begin{aligned}
\alpha_3 &= \arccos\frac{1}{\sqrt{6}} \approx 65.9052^\circ & \beta_3 &= \arccos\frac{-1}{4} \approx 104.4775^\circ \\
\alpha_4 &= \arccos\frac{1}{\sqrt{2}} = 45^\circ & \beta_4 &= \arccos\frac{1}{2} = 60^\circ \\
\alpha_5 &= \arccos\sqrt{\frac{1}{2}+\frac{1}{\sqrt{5}}} \approx 13.2825^\circ & \beta_5 &= \arccos\frac{3\phi-1}{4} \approx 15.5225^\circ
\end{aligned} \tag{42}$$

where $\phi = \frac{1+\sqrt{5}}{2}$ is the golden ratio satisfying $\phi^2 = \phi + 1$, and we used $\cos\frac{\pi}{5} = \frac{\phi}{2}$.

9.2. Shared Vertex Configuration

In a gapped 20-tetrahedron cluster, the tetrahedra are arranged with uniform angular spacing about a shared vertex; none share any edges (Figure 10). It remains true, however, that any two adjacent tetrahedra have adjacent faces which are symmetric across a mirror plane between them. Although the two faces do not themselves share an edge, the face *planes* share a common intersection line with the mirror plane (Figure 11), and the curve and twist transformations of Section 6 can be applied to bring the faces into contact.

That intersection line between the two face planes contains all points common between them, including therefore the shared vertex. Define a_i to be the unit vector directed from that vertex out to the centroid of the ith tetrahedron (its line also pass through the center of the tetrahedron's opposite, outer face—see Figure 11 again). The a_j in an adjacent tetrahedron will be the inversion of a_i through a vector n lying in the mirror plane between them.

Since the tetrahedra are evenly spaced, their 20 centroids lie at the face centers of a regular icosahedron. The angle $2\theta_M$ between adjacent a_i is then supplementary to the icosahedron's dihedral angle of $\arccos\frac{-\sqrt{5}}{3}$, or $\cos 2\theta_M = \frac{\sqrt{5}}{3}$. Furthermore, the angle θ_F from an a_i to an adjacent face in its own tetrahedron is complementary to the tetrahedron's dihedral angle of $\arccos\frac{1}{3}$, so $\sin\theta_F = \frac{1}{3}$. Equations (13) and (27) then give

$$\cos\alpha = \frac{\tan\theta_F}{\tan\theta_M} = \frac{\sin\theta_F}{\cos\theta_F}\frac{1+\cos 2\theta_M}{\sin 2\theta_M} = \frac{1}{\sqrt{8}}\frac{1+\frac{\sqrt{5}}{3}}{\frac{2}{3}} = \frac{1}{\sqrt{8}}\frac{3+\sqrt{5}}{2} \tag{43}$$

$$\cos\beta = 2\frac{\cos^2\theta_M}{\cos^2\theta_F} - 1 = \frac{1+\cos 2\theta_M}{\cos^2\theta_F} - 1 = \frac{1+\frac{\sqrt{5}}{3}}{\frac{8}{9}} - 1 = \frac{1+3\sqrt{5}}{8}. \tag{44}$$

These results may also be expressed in terms of the golden ratio ϕ, so we write

$$\alpha = \arccos\frac{\phi^2}{\sqrt{8}} \approx 22.2388^\circ, \qquad \beta = \arccos\frac{3\phi-1}{4} \approx 15.5225^\circ \tag{45}$$

for the vertex-sharing uniformly gapped 20-tetrahedron cluster. These values should be compared with those given in Table 1, which were determined by a sequence of trigonometric calculations. The 20-group considered here contains the same arrangement as the 5-fold group vertex-sharing configuration in the table; α here corresponds to V and B, and β corresponds to F.

9.3. Other Vertex-Sharing Configurations

If we start with 4 vertex-sharing tetrahedra, the most symmetric configuration in 3D is to put the centroid of each at the face center of a large tetrahedron. There is then 3-fold symmetry around an axis, so we call it the 3-fold vertex-sharing configuration (see the entry in Table 1). The angle $2\theta_M$ between centroid axes is supplementary to the dihedral angle $\arccos\frac{1}{3}$ of the large tetrahedron, or $\cos 2\theta_M = -\frac{1}{3}$; θ_F is the same as before, $\sin\theta_F = \frac{1}{3}$. Then

$$\cos\alpha = \frac{\sin\theta_F}{\cos\theta_F}\frac{1+\cos 2\theta_M}{\sin 2\theta_M} = \frac{1}{\sqrt{8}}\frac{1-\frac{1}{3}}{\frac{\sqrt{8}}{3}} = \frac{1}{4} \tag{46}$$

$$\cos\beta = \frac{1+\cos 2\theta_M}{\cos^2\theta_F} - 1 = \frac{1-\frac{1}{3}}{\frac{8}{9}} - 1 = -\frac{1}{4}. \tag{47}$$

For 4-fold symmetry, we use two layers of 4 tetrahedra each, and their centroids lie in the face centers of an octahedron. The angle $2\theta_M$ between centroid axes is supplementary to the octahedron's dihedral angle $\arccos\frac{-1}{3}$, so $\cos 2\theta_M = \frac{1}{3}$, and θ_F is still the same. Thus

$$\cos\alpha = \frac{\sin\theta_F}{\cos\theta_F}\frac{1+\cos 2\theta_M}{\sin 2\theta_M} = \frac{1}{\sqrt{8}}\frac{1+\frac{1}{3}}{\frac{\sqrt{8}}{3}} = \frac{1}{2} \tag{48}$$

$$\cos\beta = \frac{1+\cos 2\theta_M}{\cos^2\theta_F} - 1 = \frac{1+\frac{1}{3}}{\frac{8}{9}} - 1 = \frac{1}{2}. \tag{49}$$

These angles may again be compared with Table 1, for the 3- and 4-fold cases. (There is a sign difference for $\cos\beta$; this is because β here represents the exterior dihedral angle, while the values for V and B in the table represent its supplement, the interior angle.)

10. Summary and Outlook

We have discussed how the geometric frustration arising from the failure of regular tetrahedra to tile 3D space can be encoded in four different ways, arranging the tetrahedra with local symmetry that can be propagated globally to form quasicrystals. These four arrangements make symmetric use of gaps, distortion, discrete 4D curvature, and twisting, respectively, to create local order. The latter three methods bring faces of adjacent tetrahedra into contact so that the total number of independent

face planes in a cluster has a minimum value, but the latter two share the property with the gap method that the tetrahedra remain regular.

Indeed, the twist and the discrete curvature arrangements can be obtained from the gap arrangement by simple rotations, and we have found that the transformation angle in the two cases is the same, as is the relative joint angle between adjacent tetrahedra after the rotation. This match suggests the possibility of using twist to encode curvature.

A 3D Riemannian manifold, curved in 4D, can be approximated by a simplicial manifold—essentially, a triangulation of the manifold by tetrahedra (3-simplices). Perhaps such a manifold could be flattened out into a single 3-space, with twists of the tetrahedra replacing the bends to 4D, and twisted joint angles between them in flat 3-space representing the 4D folded dihedral joint angles of the original manifold. In this paper we have demonstrated this possibility locally for a vertex point of uniform curvature surrounded by regular tetrahedra, but a general simplicial manifold may have varying dihedral angles, as well as irregular tetrahedra, around a single vertex. It remains to be seen whether an arbitrary vertex can be represented by a twist configuration.

Such full generality, however, may not be required for realistic physical models. In this regard it is worth mentioning the success of Causal Dynamical Triangulation (CDT) in approximating vacuum solutions of Einstein's field equations [22] with a Feynman path integral sum of simplicial manifolds [23,24]. What is striking about this approach is the simplicity of using only (pseudo) regular 4-simplices of uniform size: all the variability of the manifold is contained in the dihedral angles at their interfaces. For a given arrangement of 4-simplices, these angles encode the geometric frustration, and hence the curvature, which is extracted by a Regge calculus operator. We have shown analogous approaches to expressing geometric frustration via our quasicrystalline formalism. As opposed to the continuous degrees of freedom CDT allows for the dihedral angles, our approach is simpler in its highly restricted sets of values, whether that be rotation, edge contraction, etc. It remains an open question as to whether or not our approach will lead to realistic Einstein field equation approximations.

To answer that question, further work will need to go beyond individual vertices and address the connections between successive vertices. It is certainly true that the projection of a corrugated layer in an nD lattice, via an irrational angle to $(n-m)$D, where $n > m$ and $n, m\mathbb{Z}$, does encode transdimensional geometrical frustration in the projection—the quasicrystal. On a Riemannian manifold, the constraint of smoothness connects local structure to its neighborhood, with implications for the global structure, and these connections are analyzed using the tools of differential geometry. For a simplicial manifold, the constraint that connects local structure to its neighborhood lies in certain regularity conditions—e.g., the triangulation must be complete (no gaps) and pure (no isolated faces or edges)—and this again has implications for the global structure. In this case, our analytic tool is the Regge Calculus. Now, for a twist configuration, Fang has shown [10,13] that the structure can be propagated globally, but one has yet to characterize the nature of connections between neighboring vertices and construct a Regge-type calculus to analyze the aggregate twist structure.

Yet another question is how a twist network would encode the properties of a Lorentzian metric. Evidently, there is much still to be done, but such a program holds out the interesting possibility of modeling spacetime itself as a flat-space quasicrystalline network of twisted simplices, with the twist taking on the traditional role of curvature.

Supplementary Materials: Provide link to Wolfram demo site.

Acknowledgments: This work was funded by Quantum Gravity Research, Los Angeles, CA, U.S.A.

Author Contributions: Klee Irwin conjectured the isomorphism between the discrete curvature and the twisting; Fang Fang and Richard Clawson carried out the research. Fang Fang discovered the proof of Klee?s conjecture as well as the different methods of encoding the geometric frustration; Richard Clawson independently proved Klee?s conjecture using Clifford algebra; Fang Fang wrote the Section 1-4 of the paper; Richard Clawson wrote Section 5-9; All three authors contributed to the writing of the conclusion.

Conflicts of Interest: "The authors declare no conflict of interest."

Abbreviations

The following abbreviations are used in this manuscript:

CDT Causal Dynamical Triangulation

Appendix A

Appendix A.1

The appendix is an optional section that can contain details and data supplemental to the main text. For example, explanations of experimental details that would disrupt the flow of the main text, but nonetheless remain crucial to understanding and reproducing the research shown; figures of replicates for experiments of which representative data is shown in the main text can be added here if brief, or as Supplementary data. Mathematical proofs of results not central to the paper can be added as an appendix.

Appendix B

All appendix sections must be cited in the main text. In the appendixes, Figures, Tables, etc. should be labeled starting with 'A', e.g., Figure A1, Figure A2, etc.

References

1. Sadoc, J.F.; Mosseri, R. *Geometric Frustration*; Cambridge University Press, 1999.
2. Chen, E.R.; Engel, m.; Glotzer, S.C. Dense crystalline dimer packings of regular tetrahedra. *Discrete and Computational Geometry* **2010**, *44*, 253–280.
3. Jaoshvili, A.; Esakia, A.; Porrati, M.; Chaikin, P.M. Experiments on the Random Packing of Tetrahedral Dice. *Physical Review Letters.* **2010**, *104*, 185501.
4. Chen, E.R. A Dense Packing of Regular Tetrahedra. *Discrete and Computational Geometry* **2008**, *40*, 214–240.
5. Cohn, H. Mathematical physics: A tight squeeze. *Nature* **2009**, *460*, 876–879.
6. Torquato, S.; Jiao, Y. Analytical Constructions of a Family of Dense Tetrahedron Packings and the Role of Symmetry. *arXiv:0912.4210* **2009**.
7. Haji-Akbari, A.; Engel, M.; Keys, A.S.; Zheng, X.; Petschek, R.G.; Palffy-Muhoray, P.; Glotzer, S.C. Disordered, quasicrystalline and crystalline phases of densely packed tetrahedra. *Nature* **2009**, *462*, 773–777.
8. Kallus, Y.; Elser, V.; Gravel, S. Dense Periodic Packings of Tetrahedra with Small Repeating Units. *Discrete and Computational Geometry* **2010**, *44*, 245–252.
9. Torquato, S.; Jiao, Y. Dense packings of the Platonic and Archimedean solids. *Nature* **2009**, *460*, 876–879.
10. Fang, F.; Kovacs, J.; Sadler, G.; Irwin, K. An Icosahedral Quasicrystal An Icosahedral Quasicrystal as a Packing of Regular Tetrahedra. *ACTA Physica Polonica A* **2014**, *126*, 458–460.
11. Elser, V.; Sloane, N.J.A. A highly symmetric four-dimensional quasicrystal. *J. Phys. A* **1987**, *20*, 6161–6168.
12. Peters, J.; Trebin, H.R. Tetracoordinated quasicrystals. *Physical Review B* **1991**, *43*, 1820.
13. Fang, F.; Irwin, K. An Icosahedral Quasicrystal as a Golden Modification of the Icosagrid and its Connection to the E8 Lattice. *arXiv:1511.07786* **2015**.
14. Fang, F.; Irwin, K.; Kovacs, J.; Sadler, G. Cabinet of curiosities: the interesting geometry of the angle $\beta = \arccos((3\phi - 1)/4)$. *ArXiv:1304.1771* **2013**.
15. Fuller, R.B. *Synergetics: Explorations in the Geometry of Thinking*; Macmillan Publishing Co., Inc, 1982.
16. Hestenes, D. Oersted Medal Lecture 2002: Reforming the mathematical language of physics. *American Journal of Physics* **2003**, *71*, 104–121.
17. Dorst, L.; Mann, S. Geometric algebra: a computational framework for geometrical applications. *IEEE Computer Graphics and Applications* **2002**, *22*, 24–31.
18. Mann, S.; Dorst, L. Geometric algebra: a computational framework for geometrical applications. 2. *IEEE Computer Graphics and Applications* **2002**, *22*, 58–67.

19. Hestenes, D.; Holt, J.W. Crystallographic space groups in geometric algebra. *Journal of Mathematical Physics* **2007**, *48*, 023514.
20. Doran, C.; Lasenby, A. *Geometric algebra for physicists*; Cambridge University Press, 2003.
21. Dorst, L.; Fontijne, D.; Mann, S. *Geometric algebra for computer science: an object-oriented approach to geometry*; Morgan Kaufmann Publishers Inc., 2009.
22. Ambjørn, J.; Jurkiewicz, J.; Loll, R. The self-organized de Sitter universe. *International journal of modern physics D* **2008**, *17*, 2515–2520.
23. Ambjørn, J.; Jurkiewicz, J.; Loll, R. The universe from scratch. *Contemporary Physics* **2006**, *47*, 103–117.
24. Ambjørn, J.; Jurkiewicz, J.; Loll, R. Causal dynamical triangulations and the quest for quantum gravity. *Foundations of Space and Time: Reflections on Quantum Gravity* **2012**, p. 321.